

Alireza REZVANI, Ali ESMAEILY, Hasan ETAATI, Mohammad MOHAMMADINODOUSHAN

# Intelligent hybrid power generation system using new hybrid fuzzy-neural for photovoltaic system and RBFNSM for wind turbine in the grid connected mode

© Higher Education Press and Springer-Verlag Berlin Heidelberg 2017

**Abstract** Photovoltaic (PV) generation is growing increasingly fast as a renewable energy source. Nevertheless, the drawback of the PV system is intermittent because of depending on weather conditions. Therefore, the wind power can be considered to assist for a stable and reliable output from the PV generation system for loads and improve the dynamic performance of the whole generation system in the grid connected mode. In this paper, a novel topology of an intelligent hybrid generation system with PV and wind turbine is presented. In order to capture the maximum power, a hybrid fuzzy-neural maximum power point tracking (MPPT) method is applied in the PV system. The average tracking efficiency of the hybrid fuzzy-neural is incremented by approximately two percentage points in comparison with the conventional methods. The pitch angle of the wind turbine is controlled by radial basis function network-sliding mode (RBFNSM). Different conditions are represented in simulation results that compare the real power values with those of the presented methods. The obtained results verify the effectiveness and superiority of the proposed method which has the advantages of robustness, fast response and

good performance. Detailed mathematical model and a control approach of a three-phase grid-connected intelligent hybrid system have been proposed using Matlab/Simulink.

**Keywords** photovoltaic, wind turbine, hybrid system, fuzzy logic controller, genetic algorithm, RBFNSM

## 1 Introduction

As the energy demand increases, more attention is paid to alternative energy sources. Renewable energy is great in energy saving, lower environmental impacts, generally better investment options, improved power security and etc. Two modern renewable energy technologies which are most promising are the wind and solar power generation. However each of these has its own drawbacks. The purpose of hybrid system is to increase the reliability of the system for overcoming uncertainty, intermittency and insufficiency of each renewable energy sources [1–5]. Wind power in distribution generation technology because of its mature technology, low cost and good efficiency can be integrated into the PV generation system to form a hybrid PV/wind generation system, which can be more stable and reliable [6]. In this paper, a study is conducted of intelligent PV/wind hybrid power system used in the grid connected mode.

In recent decade, a lot of researches have been done focusing on three types of maximum wind power extraction techniques, namely tip speed ratio (TSR) control, power signal feedback (PSF) control, and hill-climb searching (HCS) control. The rotor speed of wind turbine is regulated using the TSR control to keep an optimal TSR. The PSF control needs the comprehension of the maximum power curve of wind turbines, and keeps this curve through its control mechanisms. In the recent decade, wind turbine MPPT strategies have been devel-

Received May 6, 2016; accepted July 4, 2016

Alireza REZVANI (✉)

Department of Electrical Engineering, Saveh Branch, Islamic Azad University, Saveh 3919715179, Iran  
Water and Power Resources Development Company (IWPCO), Iran  
E-mail: alireza.rezvani.saveh@gmail.com

Ali ESMAEILY

Department of Electrical Engineering, Karaj Branch, Islamic Azad University, Karaj 3148635731, Iran

Hasan ETAATI

Iran Water and Power Resources Development Company (IWPCO), Iran

Mohammad MOHAMMADINODOUSHAN

Department of Electrical Engineering, Science and Research Branch, Islamic Azad University, Tehran 1477893855, Iran

oped. The difficulty in turbine speed measurements and wind speed leading to the TSR direction control technique is limited [6]. Radial basis function network (RBFN) is capable of learning, parallel computing, fault tolerance, and approximating any intricate nonlinearity infinitely. Sliding mode variable control is taken as a special discontinuous nonlinear control method, which has powerful robustness versus load perturbations, parameter changes and uncertainty of system, with the superiority of quickness and easy comprehension. Incorporating ANN with sliding mode variable control not only has powerful robustness which can withstand system disorder and outer interference but also removes the buffeting. In this paper, a RBFNSM-based TSR MPPT technique is applied for the wind turbine system [7].

The drawback of the PV system is intermittent because of depending on weather conditions. To track the incessantly diverging maximum power point (MPP) of the solar array, the MPPT control method plays a significant role in the PV arrays. The most common method for MPPT is the perturb-and-observe (P&O) algorithm [3], incremental conductance (IC) [4], fuzzy logic controller (FLC) [8], an artificial neural network (ANN) [9,10].

Simplicity and easy execution of the P&O method in MPPT application makes it a common method [3–5]. The drawback of this technique is the low accuracy in steady-state condition. The perturbation operation would cause an oscillation in the PV module around the MPP which results in energy wastes. By minimizing the perturbation step size, variation can be reduced but it is not assumed to be very small since a too small step size decelerates the speed of MPPT and decreases the efficiency. In addition, any prompt change in weather condition upsets the output power and the method fails to easily track the MPP.

Tracking the MPP of the PV module using fuzzy logic control (FLC) is becoming popular in the last decade. This is due to the robustness and simplicity in design since there is no need for a super accurate mathematical modelling [3,8,9]. Also, as per Refs. [8,9], on account of an optimized perturbation, the FLC based P&O and hill climbing MPPT methods have better performance. Nevertheless, careful selection of parameters, membership functions and fuzzy rules are substantial to FLC. FLC can be effective if parameters and membership functions are chosen through experimentation along with an expert opinion. Another drawback of FLC is the high cost of implementation due to the complexity of its algorithms.

New methods such as ANN have been utilized to overcome the downsides [10–13]. Since the ANN has the capability of being used on nonlinear tasks, its application in different areas has been growing. ANN does not require reprogramming since it is based on learning process.

In Ref. [14], the FLC and ANN application on PV systems as two methods of MPPT have been presented. The inputs to the two MPPT controllers are irradiance and

temperature of the PV cell which estimates the optimum duty cycle corresponding to MPP as output.

The conventional algorithms do not trap into local minimum. Such advantages distinguish the GA from the conventional algorithms. Combining ANN and the GA with the purpose of performance improvement has been presented in Ref. [13]. In this paper, the GA application is to boost the MPPT efficiency of a photovoltaic module on an induction motor drive. This can be done by enhancing the input dataset for a neural network model of the PV modules. A variable frequency volts-per-hertz (V/f) control technique is used to control the speed of the induction motor, and a space-vector pulse-width modulation (SV-PWM) method is utilized to act as a 3-phase inverter.

In Refs. [2–5,15–17], the GA has been employed in data optimization, thus the optimum values are applied for the purpose of ANN training. The outcome indicates that this technique has less fluctuation when comparing to the conventional methods. The advantages of this method operate in MPPT but there are many drawbacks in comparison with the neural network.

Reference [16] has presented a new hybrid fuzzy-neural MPPT controller. The training data of ANN are optimized using the GA. A novel GA technique to accomplish the MPPT based on the cell model has also been presented in Ref. [18].

Some works on hybrid systems have been conducted. Dynamical simulation of PV/Wind systems have been investigated for a stand-alone mode including of different wind turbine and PV array systems in Ref. [19]. It is suggested to apply particular devices for battery storage, so that incessant electricity output over the whole year may be attained. Modelling and simulation of PV/wind/battery hybrid systems connected to a grid have been discussed in Ref. [20]. It is found that in order to capture the maximum power the MPPT can be used for both wind turbine and photovoltaic panel. In Ref. [21], the hybrid PV/wave standalone energy conversion system with battery energy storage has been discussed. In this system, the bidirectional buck-boost DC-DC converter (BBDC) is applied to keep the constant DC-link voltage. It is also noted that the extra hybrid power in the battery bank supplies this power to the system load during the shortage of hybrid power. In Ref. [22], the mathematical model of system components has been assessed to model of different renewable energy particularly wind, PV, hydro and storage devices.

The authors in Ref. [23] have proposed the performance of variable step-size P&O MPPT controller and have initially developed and validated a Matlab based photovoltaic generation system model. Then, variable step-size MPPT controllers are compared in terms of the energy captured, rise time, settling time and steady-state tracking accuracy under various operating conditions. In Ref. [24], the operation of various variable step-size P&O MPPT methods has been studied. Initially, a Matlab based PV generation system model is developed and validated.

Performance indices are also represented to enhance the reliability of the comparison.

It should be noted that the aforementioned papers are lack in evaluation of the system performance in the intelligent hybrid system and no comparison has been made between the hybrid fuzzy-neural method and the conventional methods such as P&O, IC and FLC. Such a comparison could be beneficial to indicate the high performance of this method in different environmental conditions. Hence, to the best of authors' knowledge, there is none published paper presenting such framework using intelligent hybrid method for PV system in the grid connected mode. It is noted that the results confirm the superiority and effectiveness of the proposed methods. In this paper, the hybrid fuzzy neural controller is compared with three MPPT controllers of P&O, IC and fuzzy logic to show the effectiveness and superiority of the hybrid fuzzy neural controller than the conventional controllers.

The major contributions of this paper to overcome the drawbacks of the above references can be listed as follows. First, it is worth mentioning that the present paper applies the fuzzy-neural hybrid algorithm to improve the efficiency of the PV system in the rapid changing environmental condition in the hybrid system. Second, the inputs data of the FLC for hybrid fuzzy-neural method are the change of the PV system output power ( $\Delta P_{array}$ ), the change of the PV system output voltage ( $\Delta V_{array}$ ), and the change of the reference voltage ( $\Delta V_{mpp}$ ) to be the output. Next, the GA based offline is utilized to prepare the reference voltage corresponding to the MPP. Finally, the pitch angle of the wind turbine is regulated using RBFNSM controller.

## 2 PV cell model

Several studies have been conducted on the mathematical model of the PV cell. In Ref. [24], a structure of the photovoltaic cell with double diode has been studied. This model includes of a current source representing the light flux, in parallel with two diodes. The diode presents the cell behavior in darkness. Two resistances shunt and series resistance are applied to represent internal losses. Other models are proposed to simplify the model of PV cell by using one diode. Like this last research work, a single model PV cell is utilized in this paper in order to formalize and simplify the PV cell, as shown in Fig. 1. The basic equations representing the  $I$ - $V$  characteristic of the PV cell solar model are given in Eqs. (1) and (2) [3–5].

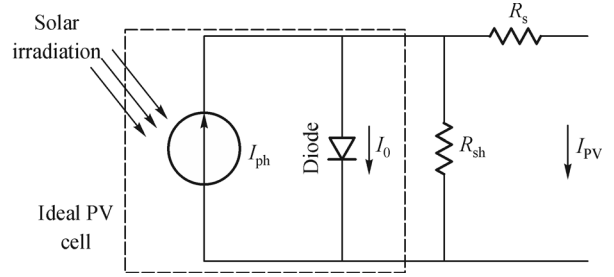


Fig. 1 Equivalent circuit of one PV array

$$I_{ph} - I_D - I_{pv} - \frac{V_{pv} + R_s I_{pv}}{R_{sh}} = 0, \quad (1)$$

$$I_D = I_0 (e^{V_D/V_T} - 1), \quad (2)$$

where

$$V_D = V_{pv} + I_{pv} R_s, \quad (3)$$

$$V_T = \frac{nKT}{q}, \quad (4)$$

where  $I_{pv}$  is the cell current (A),  $I_{ph}$  is the light generated current (A),  $I_D$  represents the Shockley diode equation (A),  $I_0$  represents the diode saturation current (A),  $R_s$  represents the cell series resistance ( $\Omega$ ),  $R_{sh}$  is the cell shunt resistance ( $\Omega$ ),  $V_D$  is the diode voltage (V),  $V_T$  represents the temperature voltage (V),  $V_{pv}$  is the cell voltage (V),  $n$  is the dimensionless junction material factor,  $K$  is the Boltzmann constant  $1.38 \times 10^{23}$  J/K,  $T$  is the temperature measured by Celsius, and  $q$  is the electron charge  $1.602 \times 10^{-19}$  C.

The Red Sun 90 W is used as the reference module and attained under the standard test condition (STC) with a solar irradiance of  $1000 \text{ W/m}^2$  and a temperature of  $25^\circ\text{C}$ . Simulations are accomplished using the Matlab/Simulink. The proposed MPPT method is developed to a 4.4 kW PV array consisting of 49 PV modules as  $7 \times 7$  array. The tracking efficiency is applied to analyze the tracking operation for different MPPT algorithms. The parameters of the solar module used (Red Sun 90 W) are given in Table 1.

The tracking efficiency is expressed as [23]

$$\eta_{mppt} = \frac{\int_{t_1}^{t_2} P dt}{\int_{t_1}^{t_2} P_{max} dt}, \quad (5)$$

Table 1 Red sun 90 W module under STC

$I_{mp}$ (Rated current) /A	$V_{mp}$ (Rated voltage) /V	$P_{max}$ (Rated power) /W	$V_{oc}$ (Open circuit voltage)	$I_{sc}$ (Short circuit current)	$N_p$ (number of parallel cells)	$N_s$ (number of series cells)
4.94	18.65	90	22.32	5.24	1	36

where  $t_1$  represents the start-up time of the system and  $t_2$  is the close-down time of the system,  $P$  is the output power of PV, and  $P_{\max}$  represents the theoretical maximum power of PV.

### 3 MPPT-GA technique

#### 3.1 Steps of implementing GA

The GA is based on the conception of the evolutionary method and prepares optimal results much faster than trial-and-error techniques. The GA uses three kinds of rules at each step to prepare the next generation from the current population: selection rules that choose the individuals, named parents and contribute to the population at the next generation; crossover rules that merge two parents to form children for the next generation; and mutation rules that use random changes to individual parents to form children.

The GA is utilized based on the offline mode to deliver the reference voltage ( $V_{\text{mpp}}$ ) which is corresponding to the maximum power. The optimum values generated out of the GA is utilized for training network [3–5,15–18]. The procedure of the GA can be found in Refs. [3–5]. Design variable can be considered as  $x$  equal to array current ( $I_x$ ) and moreover,  $F_x$  represents the output power of array which should be maximized [3–5]. Table 2 lists the GA structures.

$$F_x = V_x I_x, \quad (6)$$

$$V_x = n_s \left[ v_0 - \frac{R_s}{n_p} I_x + \frac{nk(T + 273)}{q} \ln \left( \frac{I_{\text{PV}} - I_x/n_p + I_0}{I_0} \right) \right]. \quad (7)$$

The power should be set based on the  $I_x$  to assign the objective function

$$F_x = n_s \left[ v_0 - \frac{R_s}{n_p} I_x + \frac{nk(T + 273)}{q} \ln \left( \frac{I_{\text{PV}} - I_x/n_p + I_0}{I_0} \right) \right] I_x, \quad (8)$$

where

$$0 < I_x < I_{\text{sc}}. \quad (9)$$

As a result of maximizing  $F_x$ ,  $V_{\text{mpp}}$  and MPP will be produced in any specific conditions. The GA receives 390 sample data (irradiance between 50 to 1000 W/m<sup>2</sup> and temperatures between 5°C to 55°C) to obtain the optimal voltage. The obtained results are compared with real values, which shows a negligible error of about 0.0002%.

#### 3.2 Enhancement of MPPT by combination of fuzzy-neural algorithm

The fuzzy logic and ANN methods have significant benefits when comparing to the conventional techniques; nevertheless ANN has disadvantages such as dependency to its parameters. The fuzzy logic method requires a trade-off to be done between the tracking time and static error. The ANN controller is dependent on time, training error and estimation of non-linear functions. By combining these two techniques, the above mentioned problems will be resolved effectively [16]. The diagram of the discussed method is illustrated in Fig. 2(a).

As shown in Fig. 2(b) the  $P$ - $V$  characteristic is divided into two regions. When the PV operation point is located at the first region, far from MPP, it can be redirected towards the second region, the vicinity of MPP, using ANN only [16]. In the second region, the PV operation point is adjacent to the MPP, excluding the cases when the feature of the PV system is changed. Thus, by minor changes in the PV system voltage by fuzzy controller, the operation point will be put precisely on the MPP. The flowchart of these two stages is demonstrated in Fig. 3. Using this method, the two major downsides of the ANN (time dependence) and the fuzzy logic (trade-off) will be resolved. The details of the hybrid fuzzy-neural method have been described in Ref. [16].

##### 3.2.1 Neural network

The most appropriate method of anticipating the nonlinear systems is ANN. Non-linear systems can be estimated by multi-layer neural networks which has better outcome in comparison to other methods. ANN is a novel structure applied in solving a wide kind of works that are difficult to handle ordinary rule-based programming, containing computer vision, pattern and speech recognition, identification, classification and control systems. ANN is simple, fast, and highly accurate. Generally, the ANN method has three important stages. In this paper, the feed forward neural network for MPPT process control is implemented. The core structure of ANN is based on the fact that the training process requires data to be acquired on each PV system and each specific position [3–5,15–17].

##### 3.2.2 Fuzzy control

Inputs data of the fuzzy logic controller are the change of the PV system output power ( $\Delta P_{\text{array}}$ ), the change of the PV system output voltage ( $\Delta V_{\text{array}}$ ) and the change of the

**Table 2** Genetic algorithm parameters

Number of design variable	Population size	Crossover constant/%	Mutation rate/%	Maximum generations
1	20	80	10	20

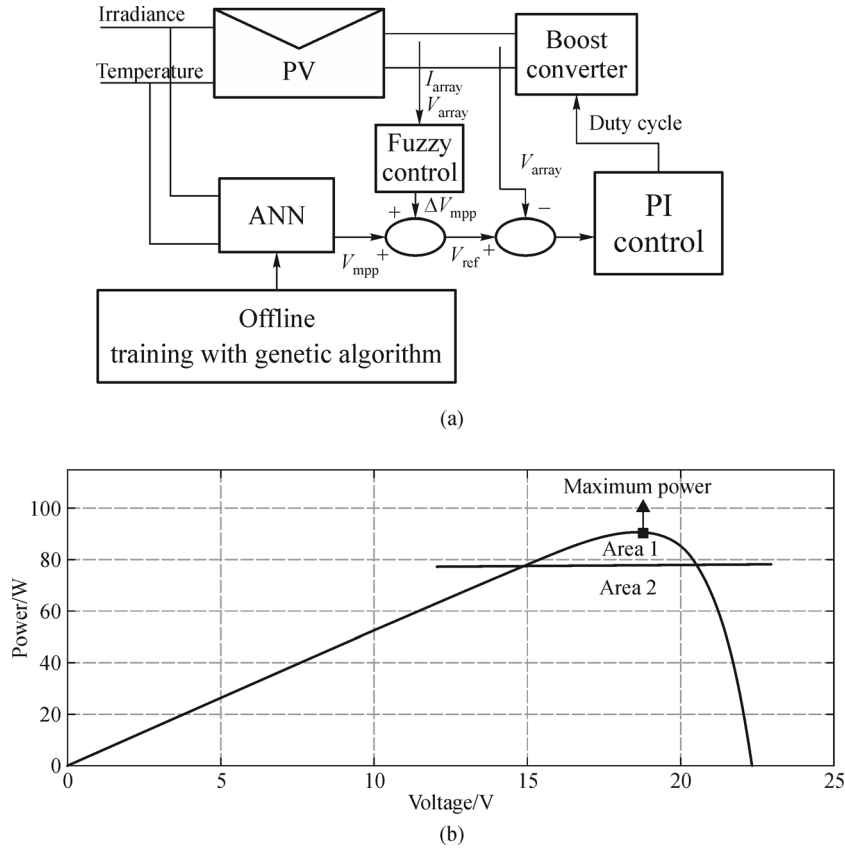


**Fig. 2** Diagram of the discussed method  
 (a) Proposed MPPT Scheme in PV system; (b)  $P-V$  characteristic that is separated into two areas

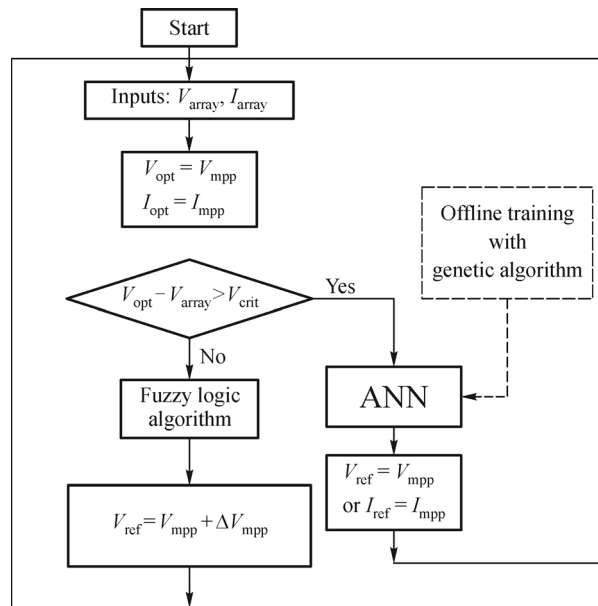


**Fig. 3** Structure of fuzzy-neural hybrid method

reference voltage ( $\Delta V_{mpp}$ ) to be the output.

Figure 4 depicts the membership functions. Also, for Centroid, the Min-Max technique is taken into account as a

defuzzification mechanism. Table 3 tabulates the required guidelines implemented to acquire the best results, where linguistic variables are presented as positive (P), negative

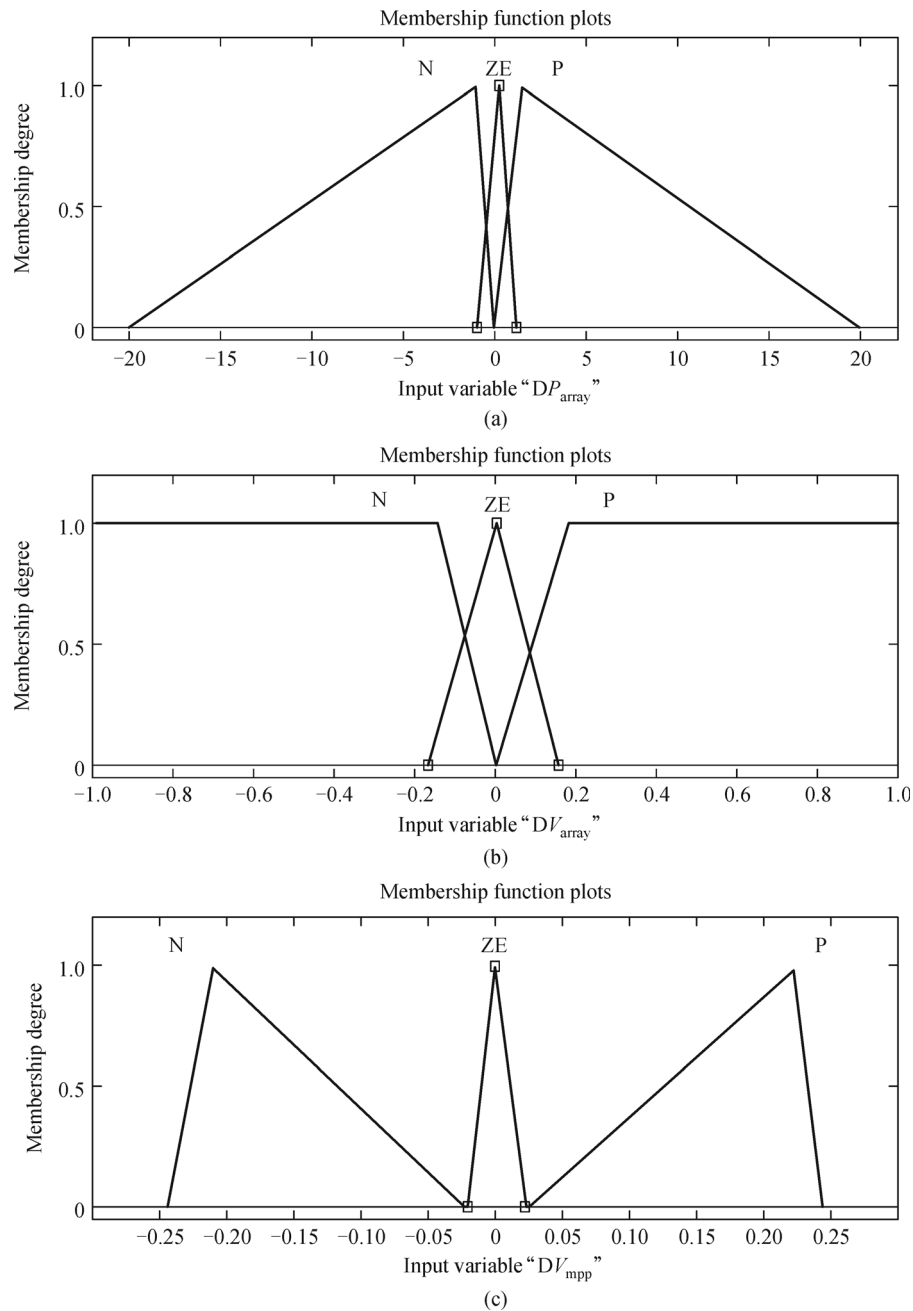


**Fig. 4** The membership function of fuzzy logic

(a) Membership functions of  $DP_{array}$ ; (b) Membership functions of  $DV_{array}$ ; (c) Membership functions of  $DV_{mpp}$

**Table 3** Fuzzy rules

Rule number	$\Delta P_{pv}$	$\Delta V_{pv}$	$\Delta_{ref}$
1	P	P	P
2	P	N	N
3	N	P	N
4	N	N	P
5	P	P	P

(N) and zero (ZE). In Ref. [16], supplementary information of the fuzzy method, which is used in this paper, has been presented.

## 4 Wind turbine model

The kinetic energy of wind is converted to electrical energy through a WT. Control objectives determine the level of simulation intricacy of WTs. When modeling a WT,

complicated simulators are needed for verification of dynamic response of aerodynamic loading and multiple components. In general, interaction of large components and dynamic loads are verified by an aero elastic simulator. Simplified mathematical models can be used instead of complex simulators to design a WT controller. A set of nonlinear ordinary differential (OD) equations with restricted degree of freedom are utilized in this work for modeling WT. The nonlinear expression for the captured aerodynamic power by the rotor is given in Eq. (10) [7].

$$P_a = \frac{1}{2}\pi\rho R^2 C_p(\lambda, \beta) v^3. \quad (10)$$

It can be easily seen from Eq. (10) that the aerodynamic power  $P_a$  has a direct relationship with cube of the wind speed. Power coefficient  $C_p$  depends on blade pitch angle  $\beta$  and tip speed ratio  $\lambda$  which is defined as

$$\lambda = \frac{\omega_r R}{v}, \quad (11)$$

which is a ratio between linear tip speed and wind speed.

In this paper, a variable-speed pitch-regulated wind turbine is studied, where the role of the angle controller is crucial.  $C_p$ - $\lambda$  curves of the wind turbine studied in this paper is displayed in Fig. 5(a) for different pitch angles [7]. As it can be seen from Fig. 5(a), adjustment of pitch angle  $\beta$  can change  $C_p$ . In other words, pitch angle control regulates the output power of the WT.

Figure 5(b) and (c) depicts the wind power system that is applied in this paper. The radial basis function network-sliding mode (RBFNSM) and proportional-integral (PI) are described in more detail in Refs. [7,25,26].

The RBFN input is considered as switching function, the output of neural network is the sliding mode controller, and the RBFNSM control is accomplished based on the self-learning ability. Figure 5(d) illustrates the model of the RBFNSM controller in Eq. (12).

$$s(t) = ce(t) + \dot{e}(t). \quad (12)$$

The reference output power and real power of the generator is represented by  $P_{ref}$  and  $P_{out}$  respectively and  $e$  represents the tracking error. Eqs. (13) to (17) explain the details of the model.

$$w_j(t) = w_j(t-1) + \eta[y(t) - y_m(t)]h_j + \alpha[w_j(t-1) - w_j(t-2)], \quad (13)$$

$$\Delta b_j = [y(t) - y_m(t)]w_j h_j \frac{\|x - c_j\|^2}{b_j^3}, \quad (14)$$

$$b_j(t) = b_j(t-1) + \eta\Delta b_j + \alpha[b_j(t-1) - b_j(t-2)], \quad (15)$$

$$\Delta b_{ij} = [y(t) - y_m(t)]w_j \frac{x_j - c_{ij}}{b_j^2}, \quad (16)$$

$$c_{ij}(t) = c_{ij}(t-1) + \eta\Delta c_{ij} + \alpha[c_{ij}(t-1) - c_{ij}(t-2)], \quad (17)$$

where  $\alpha$  and  $\eta$  represent the momentum factor and the adaptive rate, respectively.

## 5 Control strategies

The wind turbine and PV are connected to the main grid through the inverter. The inverter is applied in current control approach with PWM switching mechanism to create the inductance current and achieve a low total harmonic distortion (THD) injected current. The strategy of control mainly consists of two loops, namely a fast internal current loop and an external voltage loop. The methods of the proposed multi-level control are based on the instantaneous power on the direct-quadrature-zero ( $dq0$ ) transformation applied for PWM control [27]. The control scheme of the grid-side inverter is shown in Fig. 5(e).

### 5.1 External control loop

The external control is to keep the generated power from the PV/wind turbine to the grid constant. The active and reactive power from the grid-side inverter is defined by

$$\begin{cases} P_g = v_{ga}i_{ga} + v_{gb}i_{gb} + v_{gc}i_{gc} \\ Q_g = \frac{1}{\sqrt{3}}(v_{gab}i_{gc} + v_{gbc}i_{ga} + v_{gca}i_{gb}) \end{cases}, \quad (18)$$

where  $v_{ga}$ ,  $v_{gb}$ , and  $v_{gc}$  represent three-phase voltages at the AC bus, while  $i_{ga}$ ,  $i_{gb}$ , and  $i_{gc}$  represent the three-phase currents injected into the AC grid.

Using Park transformation as expressed in Eq. (19),

$$\begin{cases} P_g = 1.5(v_{gd}i_{gd} + v_{gq}i_{gq}) \\ Q_g = -1.5(v_{gq}i_{gd} - v_{gd}i_{gq}) \end{cases}, \quad (19)$$

where  $v_{gq}$  and  $v_{gd}$  are the  $dq$  components of the voltage at PCC, while  $i_{gq}$  and  $i_{gd}$  are  $dq$  components of the line current. In the reference frame synchronized with the grid voltage,  $v_{gq} = 0$ ,  $v_{gd} = v_g$ , thus

$$\begin{cases} P_g = 1.5v_{gd}i_{gd} \\ Q_g = -1.5v_{gd}i_{gq} \end{cases}. \quad (20)$$

Equation (20) indicates that the active and reactive power is carried by  $d$ -axis current alone and  $q$ -axis current alone, respectively. This makes the active and reactive powers to be controlled by controlling the respective currents independently. So, active and reactive powers are respectively proportional to  $i_{gd}$  and  $i_{gq}$ .

$$\begin{cases} i_{gd,ref} = \left( K_{gd,p} + \frac{K_{gd,i}}{s} \right) (V_{dc,ref} - V_{dc}) \\ i_{gq,ref} = - \left( K_{gq,p} + \frac{K_{gq,i}}{s} \right) (Q_{g,ref} - Q_g) \end{cases}, \quad (21)$$

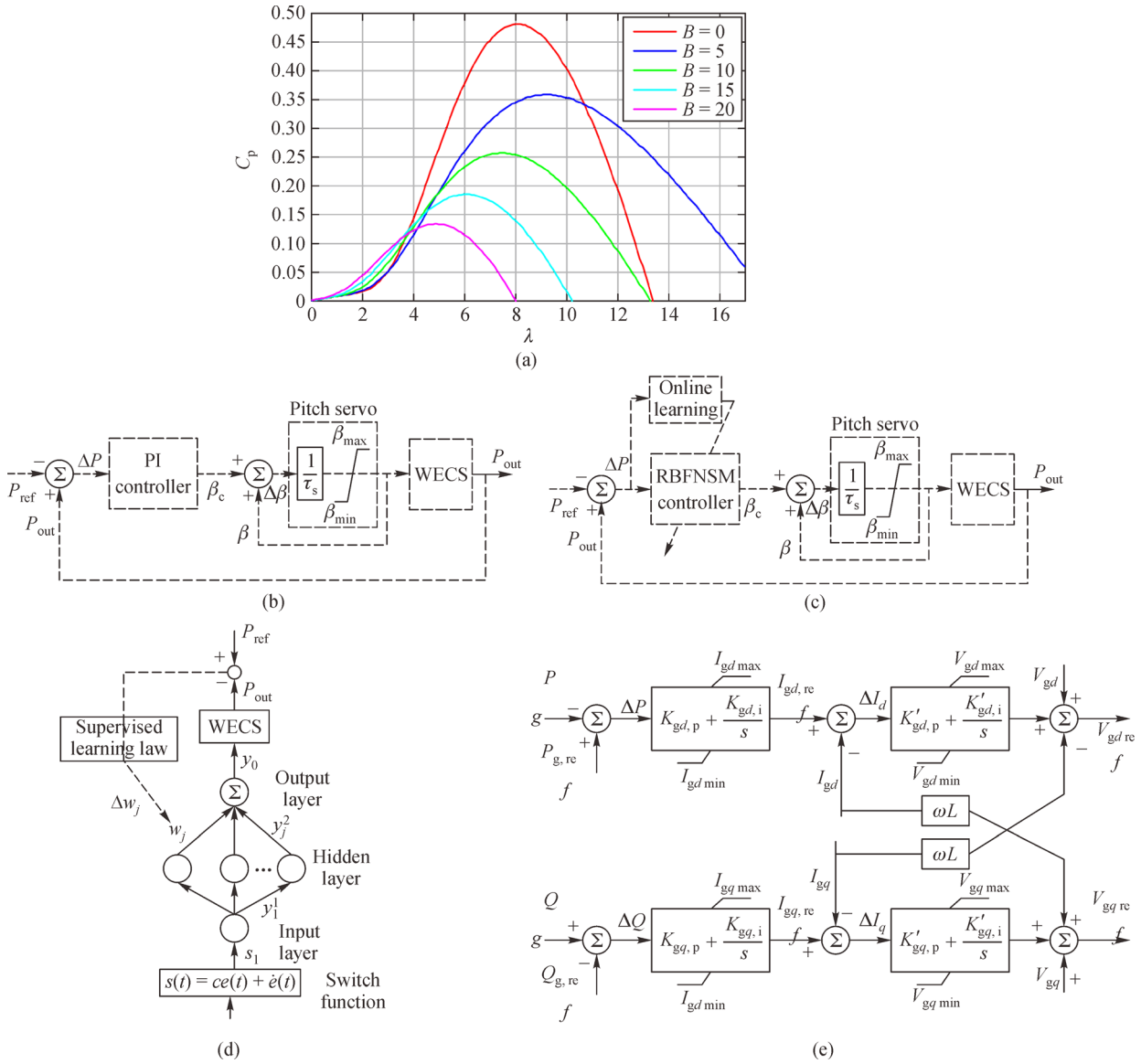


Fig. 5 Pitch angle control

(a) Power coefficient  $C_p$  ( $\lambda, \beta$ ) for various values of pitch angle  $\beta$ ; (b) PI controller; (c) RBFNSM controller; (d) structure of the RBFNSM; (e) control strategy

where  $V_{dc}$  represents the voltage of the DC link.

### 5.2 Internal control loop

It can be obtained as Fig. 5(e),

$$\begin{cases} v_{ga} = v_a - \left( L_f \frac{di_a}{dt} + R_f i_a \right) \\ v_{gb} = v_b - \left( L_f \frac{di_b}{dt} + R_f i_b \right) \\ v_{gc} = v_c - \left( L_f \frac{di_c}{dt} + R_f i_c \right) \end{cases}, \quad (22)$$

where  $v_a, v_b,$  and  $v_c$  represent the three-phase voltages at

the AC side grid, while  $L_f$  and  $R_f$  are the filter inductance and resistance respectively. In rotating the dq frame, Eq. (22) can be expressed as

$$\begin{cases} v_{gd} = v_d - \left( L_f \frac{di_d}{dt} + R_f i_d \right) + \omega L_f i_q \\ v_{gq} = v_q - \left( L_f \frac{di_q}{dt} + R_f i_q \right) - \omega L_f i_d \end{cases}, \quad (23)$$

where  $\omega$  is the grid frequency.

Let

$$\begin{cases} v'_d = L_f \frac{di_d}{dt} + R_f i_d \\ v'_q = L_f \frac{di_q}{dt} + R_f i_q \end{cases}, \quad (24)$$

then

$$\begin{cases} v_{gd} = v_d + v'_d - \omega L_f i_q, \\ v_{gq} = v_q + v'_q + \omega L_f i_d. \end{cases} \quad (25)$$

The current controller utilizes PI regulator, therefore

$$\begin{cases} v_{gd,ref} = v_d + \left( K'_{gd,p} + \frac{K'_{gd,i}}{s} \right) (i_{d,ref} - i_d) - \omega L_f i_q \\ v_{gq,ref} = v_q + \left( K'_{gq,p} + \frac{K'_{gq,i}}{s} \right) (i_{q,ref} - i_q) - \omega L_f i_d. \end{cases} \quad (26)$$

## 6 Structure of proposed system

In this paper, a case study has been conducted to show the efficiency and the effectiveness of the proposed methods using Matlab/Simulink. The proposed hybrid is formed by a PV array as a main source, a PV DC-DC boost converter, a DC bus, a wind turbine, an inverter controller and a load model. The performance of the hybrid system is to supply power to the loads.

The block diagram of the proposed system is illustrated in Fig. 6(a). The hybrid system includes a 4.4 kW PV system and a 60 kW wind turbine system. The voltage and frequency of the grid are 220 V and 60 Hz, respectively. Further information of the detailed models is reported in Appendix. The proposed MPPT technique is used to a 4.4 kW PV system composed of 49 PV modules as  $7 \times 7$  array. To show the performance of the hybrid fuzzy-neural method, simulations are performed under the following test circumstances. The structure of the grid controller is depicted in Fig. 6(b).

## 7 Simulation results and discussion

### 7.1 ANN structure

The basic configuration of the ANN is depicted in Fig. 6 (b). It is a three-layered feed forward neural network. The temperature and solar irradiance is taken as the input variables of the ANN. The  $V_{mpp}$  equivalent to MPP is the output of the ANN. To adjust the weights, the propagation algorithm and gradient descent methods are applied [6]. The algorithm propagates the error between the estimated and real output. It is noted that the output of the PV varies over the time period and climate conditions. 390 sample data (irradiance between 50 to 1000 W/m<sup>2</sup> and temperatures between 5°C to 55°C) are generated to train the network. To carry out the ANN, the layer number, the neurons number of each layer, and the transmission function of each layer should be assigned. The suggested ANN has taken into account three layers. The first and the second layers have 17 and 9 neurons, respectively, and the third layer has 1 neuron. The transfer functions of the first

and the second layers are Tansig and the third layer can be considered as Purelin. Besides, Trainlm is taken as the training function. 500 training epochs and applying training as a training function are sufficient enough to get good results. The training data is obtained by simulating the PV system in Matlab/Simulink using the genetic algorithm. The error computation is performed by the algorithm of mean square error method (MSE) during the training process. The admissible of MSE for the ANN is assigned to be  $10^{-3}$ .

The training data are presented to the network during training, and the network is adjusted according to its error. The ANN training with the target data is illustrated in Fig. 7. After the ANN has been trained, a validity test is executed. For this task, a set of samples different from those used for the training procedure is taken. The validation data are used to measure network generalization, and to stop training when best generalization is achieved. Figure 8 shows a set of 60 data for the validation data to investigate the accuracy of the results obtained from the ANN. Test data are not used in training of network. Figure 9 exhibits the random test data with 80 samples, which are not included in the training data that show a trifling testing error percentage of about 0.3%.

Figures 7–9 show the calculated MSE and regression. MSE is the average squared error difference between outputs and targets. Lower values are better. Zero means no error. Regression values measure the correlation between the outputs and targets. The value of 1 means a close relationship, and 0 a random relationship.

### 7.2 Effect of irradiance/wind speed variations

In this case, in order to assess the intelligent of the hybrid structure, the irradiance is increased from 4 to 8 s and 11 to 14 s, and it is decreased between 8 and 11 s as depicted in Fig. 10(a). In this case, the third load is not connected to the hybrid system. Distributed generation sources feed only the first and the second loads. The cell temperature is kept at a constant value of 25°C. Under these operation conditions, Fig. 10(b) depicts the performance of the MPPT controllers in terms of PV output power when subjected to a sudden change in solar irradiation. From Fig. 10(b), it can be seen that the hybrid fuzzy-neural algorithm can provide good dynamic operation, faster convergence speed, less oscillations of operating point around MPP. It tracks the global maxima under different conditions effectively than the P&O and FLC. The operating point does not vary too much from MPP under the quick changing atmospheric condition and it is more effective. The efficiency of the MPPT techniques is evaluated by considering the steady state response of the system as shown in Fig. 10(c), (d) and (e). The average tracking efficiency and respond time of each method are presented in Table 4. It can be seen that the average efficiency of the hybrid fuzzy-neural method is 99% whereas that of the

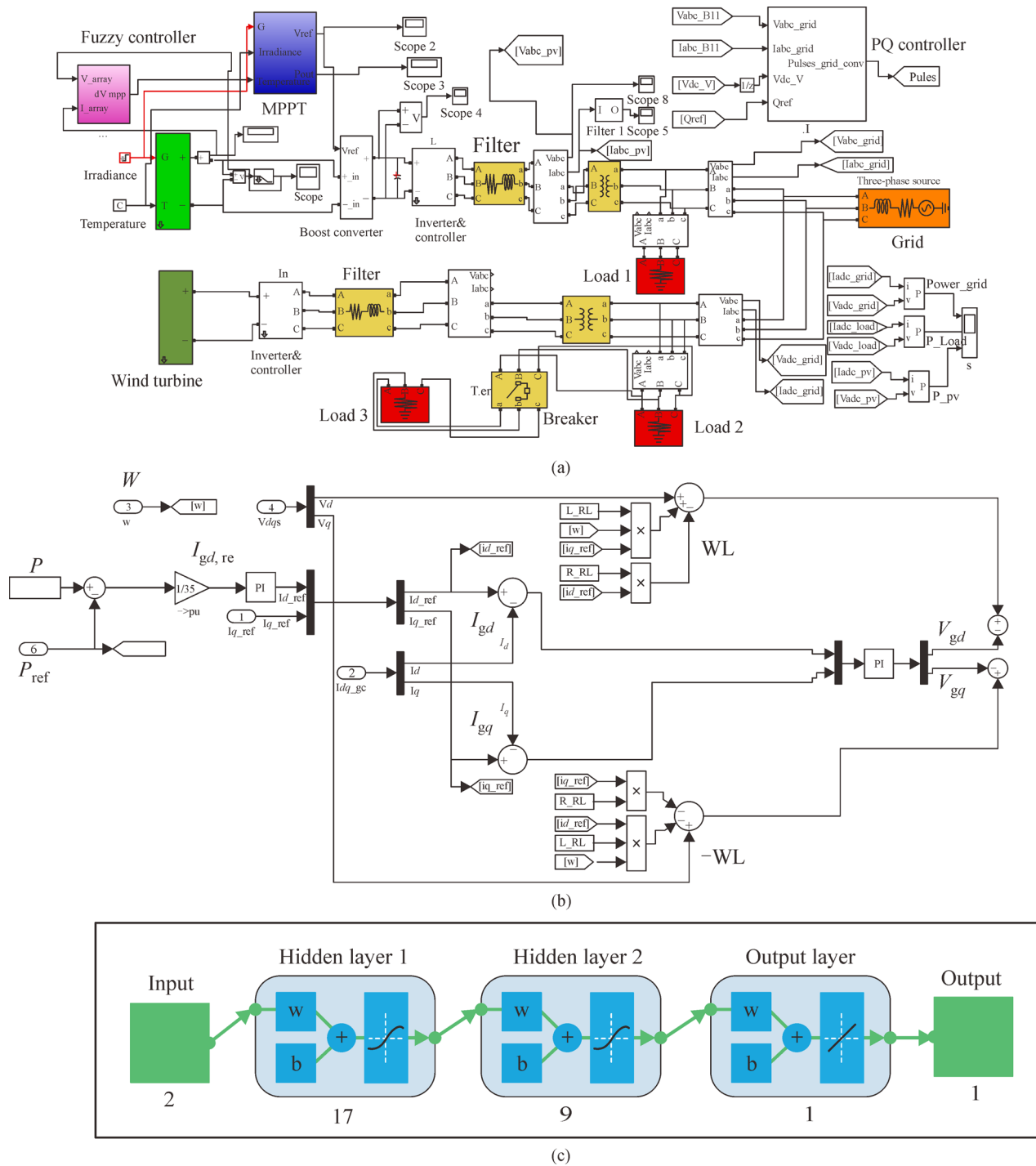


Fig. 6 Control strategy

(a) Case study system; (b) structure of P/Q strategy; (c) feed forward neural network for MPPT

P&O and FLC techniques change between 95% and 97%. It is worth mentioning that through Fig. 10(f), when the solar irradiance is 2 kW/m<sup>2</sup> and 6 kW/m<sup>2</sup>, the PV array is less than 4400 W, therefore, the grid supplies active power to the hybrid system. The output current and voltage of the PV are given in Fig. 10(g) and (h) respectively. When the

irradiance is increased to  $t = 4$  s and  $t = 11$  s, it causes an increase in the output current of the PV system. Table 5 compares the real power values with that of the presented methods in different irradiance conditions.

In addition, the dynamic responses of the wind turbine are investigated in the state of fixed load and variable wind

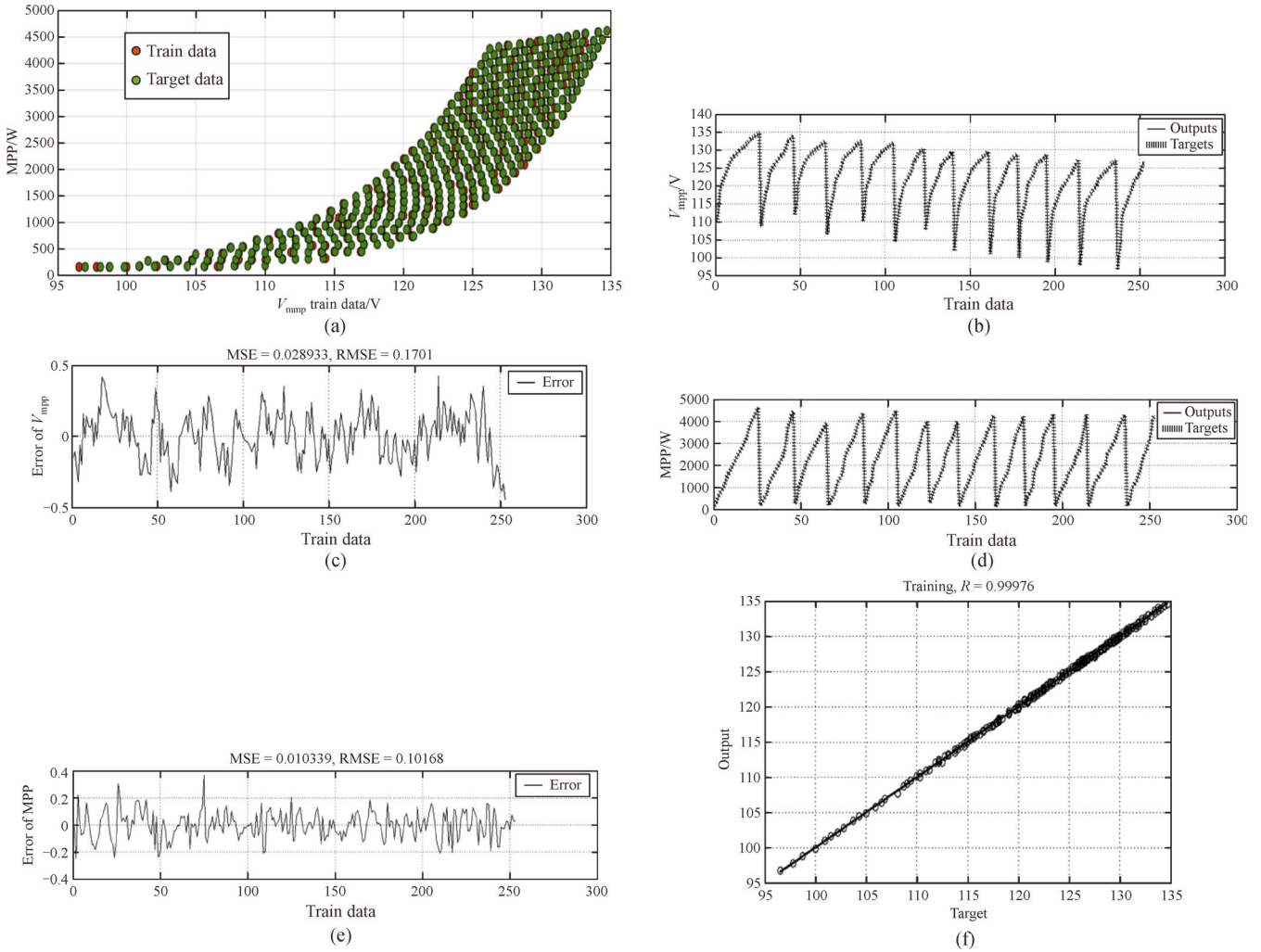


**Fig. 7** Training data of ANN controller

(a) Output of the neural network training with the amount of target data; (b) output of the neural network of  $V_{mpp}$  with the amount of data; (c) total error percentage of the  $V_{mpp}$ ; (d) output of the neural network of MPP with the amount of target data; (e) total error percentage of the MPP; (f) regression performance

speed. The wind speed during  $0 < t < 5$  is 9.5 m/s, but at  $t = 5$  s, it is reduced to 9 m/s. Then, at  $9 < t < 14$ , the wind speed is 12 m/s. Figure 11(a) demonstrates the output power from the WT. As can be noted, the RBFNSM controller provides a better operation with fewer deviations than the PI controller. It is obvious that the PI controller oscillates much more, but RBFNSM fluctuates only slightly. The wind speed is 9.5 m/s during  $0 < t < 5$  as well as it is less than 60 kW, therefore, the grid supplies power to the hybrid system as depicted Fig. 11(b). It can be seen that the active power from the grid to the hybrid system in the RBFNSM controller is less than that in the PI controller because the RBFNSM controller generates power much more than the PI controller. Figure 11(c) illustrates the inverter output current of the wind turbine.

### 7.3 Effect of temperature variation and load change

In this case assess the effect of temperature changes the evolution of the operating point of the PV array at a fixed insulation of  $1000 \text{ W/m}^2$ . Figure 12(a) shows the corresponding PV output powers during a sudden change in temperature. It is worth mentioning that the proposed hybrid fuzzy-neural method is superior to the P&O and FLC methods in tracking the MPP of the system, as shown in Fig. 12(b). It can be observed that when the cell temperature increases from  $30^\circ\text{C}$  to  $50^\circ\text{C}$ , the hybrid fuzzy-neural tracks rapidly MPP with negligible oscillations, generates maximum power, but smaller oscillation than P&O and FLC methods. However, the other MPPT techniques have some deviation from the MPP during this increase of temperature. The average tracking efficiency and time respond of each method are presented in Table 6.

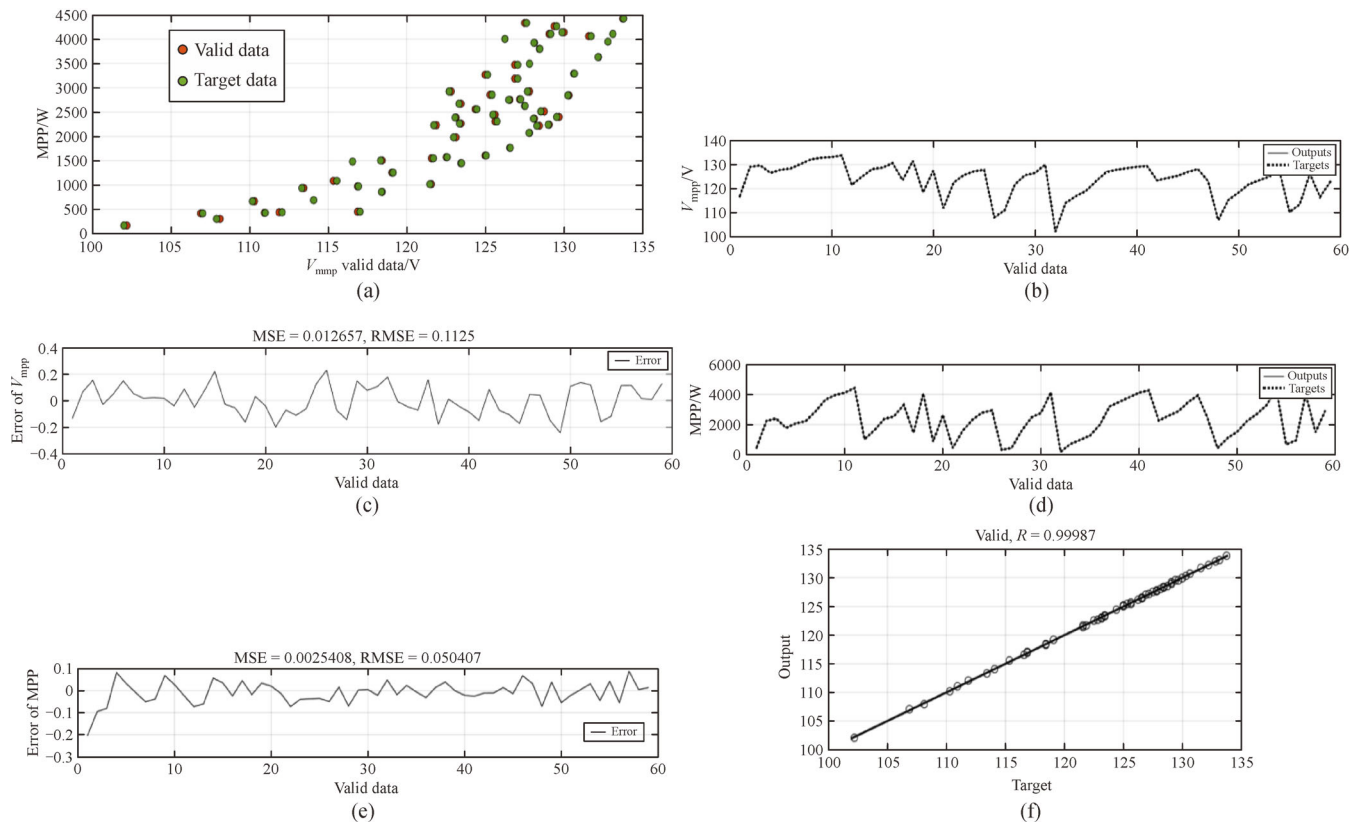


**Fig. 8** Validation data of ANN controller

(a) Output of the neural network with the amount of target data; (b) output of the neural network of  $V_{mpp}$  with the amount of valid target data; (c) percentage error of valid data  $V_{mpp}$ ; (d) output of the neural network of MPP with the amount of target data; (e) percentage error of MPP valid data; (f) regression performance

It can be derived that the average efficiency of the conventional methods vary from 95% to 97% whereas the hybrid fuzzy-neural method is 99%, as shown in Fig. 12(c), (d) and (e). Besides, the response time to achieve the MPP is also low. It can be seen from Fig. 12(f) that when the PV array is less than 4400 W, the grid supplies power to the hybrid system. The output current of the PV is depicted in Fig. 12 (g). When the temperature is increased at  $t = 4$  s, the output current of the PV system is decreased. Table 7 compares the real power values with the presented methods in different temperature conditions.

Additionally, the dynamic responses of the wind turbine are studied in the state of load change. The third load is connected to the hybrid system at  $t = 7$  s. The wind speed during  $0 < t < 14$  is 12 m/s. Figure 13(a) depicts the output power from the WT. As can be noted, the RBFNSM controller provides a better operation with fewer deviations than the PI controller. The RBFNSM algorithm tracks the maximum power more quickly and accurately than the PI controller. During load change, where the active output power of the PV and wind turbine are not sufficient, active power is provided from the grid as shown Fig. 13 (b). It can be seen that the active power from the grid to the hybrid

system in the RBFNSM controller is less than that from the PI controller because the RBFNSM controller generates much more power than the PI controller. Figure 13(c) illustrates the inverter out current of the wind turbine. Table 8 represents the performance comparison of two controllers used in the wind turbine.

## 8 Conclusions

In this paper, a dynamic modeling of intelligent hybrid photovoltaic/wind turbine system has been presented. A new method has been presented based on the hybrid fuzzy-neural MPPT of PV generation to track the MPP. The detailed mathematical model and a control approach of a three-phase grid-connected intelligent hybrid system have been proposed. The acceptable results are summarized as follows. The simulation of the hybrid system has been developed using Matlab/Simulink. Within the context of this paper, numerical simulations have been performed for the hybrid system containing intelligent fuzzy-neural, RBFNSM and conventional MPPT controllers, under varying climatic conditions. The proposed method has a

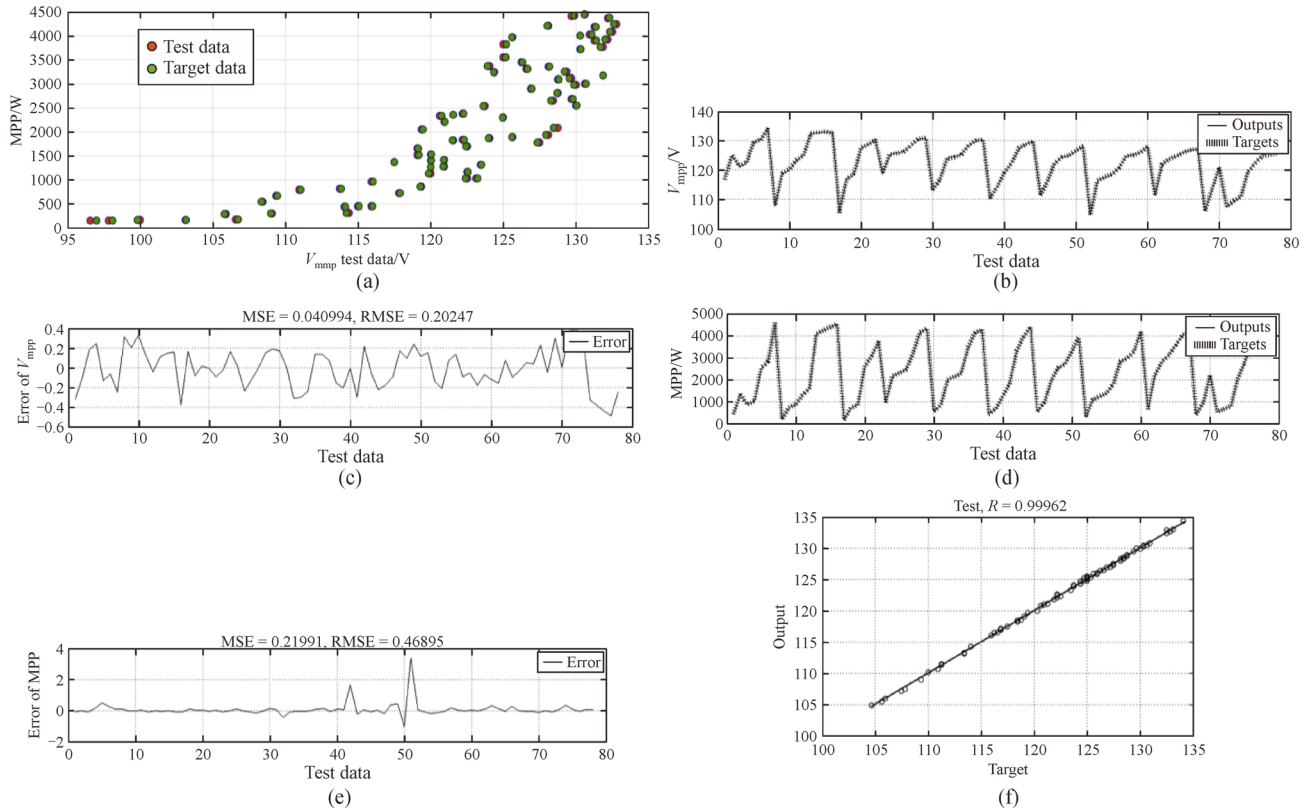


**Fig. 9** Testing data of ANN controller

- (a) Output of the neural network test with the amount of target data; (b) output of the neural network test of  $V_{mpp}$  with the amount of test target data; (c) percentage error of test data  $V_{mpp}$ ; (d) output of the neural network test of MPP with the amount of target data; (e) percentage error of MPP test data; (f) regression performance

**Table 4** Tracking efficiency and response time comparison for different MPPT techniques under irradiance variation

Algorithm	Tracking efficiency (avg)	Response time (avg)/s	Oscillation around MPP (avg)/W
Hybrid fuzzy-neural	99.12	0.10	2.52
Fuzzy logic	97.35	0.17	7.31
P&O	95.14	0.28	29.12

**Table 5** Output power values of solar array in various irradiation conditions

Time/s	Real value/W	Hybrid fuzzy-neural/W	Fuzzy logic/W	P&O/W
0–4	1600	1598	1555	1533
4–8	3530	3527	3470	3455
8–11	1600	1598	1555	1533
11–14	4400	4398	4348	4325

good dynamic performance in tracking quickly and accurately the maximum power output of the hybrid power system. The proposed method of the PV is more speedy and precise in the tracking of the MPP than the P&O and FLC methods. It is also noted that the RBFNSM in the wind turbine demonstrates better transient response, more efficiency and more stability in different conditions.

## Appendix Detailed description of the model

PV parameters: output power = 4.4 kW, carrier frequency in  $V_{MPPT}$  PWM generator = 4.3 kHz, carrier frequency in grid-side controller = 5 kHz.

Boost converter parameters:  $L = 3.5$  mH,  $C = 630$   $\mu$ F.

PI coefficients in grid-side controller:  $K_{pVdc} = 3.5$ ,  $K_{iVdc} = 7.3$ ,  $K_{pId} = 8.4$ ,  $K_{iId} = 343$ ,  $K_{pIq} = 8.4$ ,  $K_{iIq} = 343$ .

Wind turbine parameters: output power = 60 kW, stator resistance per phase = 2.8 Ω.  
 Inertia: 0.7e kg · m<sup>2</sup>, torque constant 12N-M/A, pole pairs = 8, nominal speed = 12 m/s, L<sub>d</sub>=L<sub>a</sub>= 6.3 mH.  
 Grid parameters: X/R = 7.

Other parameters: DC link capacitor = 4700 μF, DC link voltage = 950.  
 PI coefficients in grid-side controller: K<sub>pVdc</sub>=7.2, K<sub>iVdc</sub>=360, K<sub>pId</sub>=0.73, K<sub>iId</sub>=6, K<sub>pIq</sub>=0.73, K<sub>iIq</sub>=6.  
 Loads: load 1 = 4.4 kW, load 2 = 60 kW, load 3 = 15 kW.

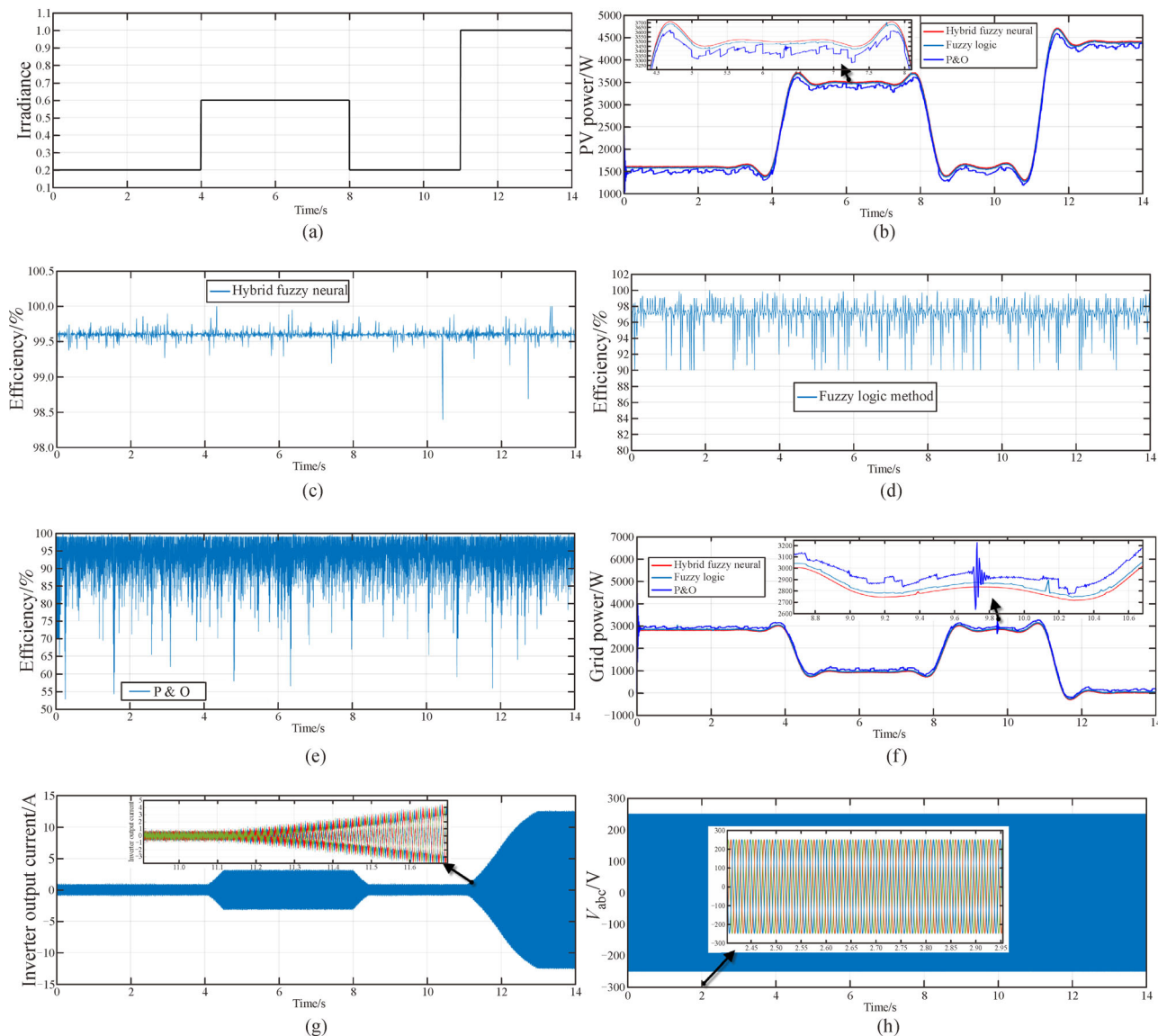


**Fig. 10** Simulated results of variations of irradiance in case 1

(a) Irradiance variations; (b) output power of PV system; (c) tracking efficiency of hybrid fuzzy-neural; (d) tracking efficiency of FLC; (e) tracking efficiency of P&O; (f) grid power; (g) inverter output current; (h) inverter output voltage of PV

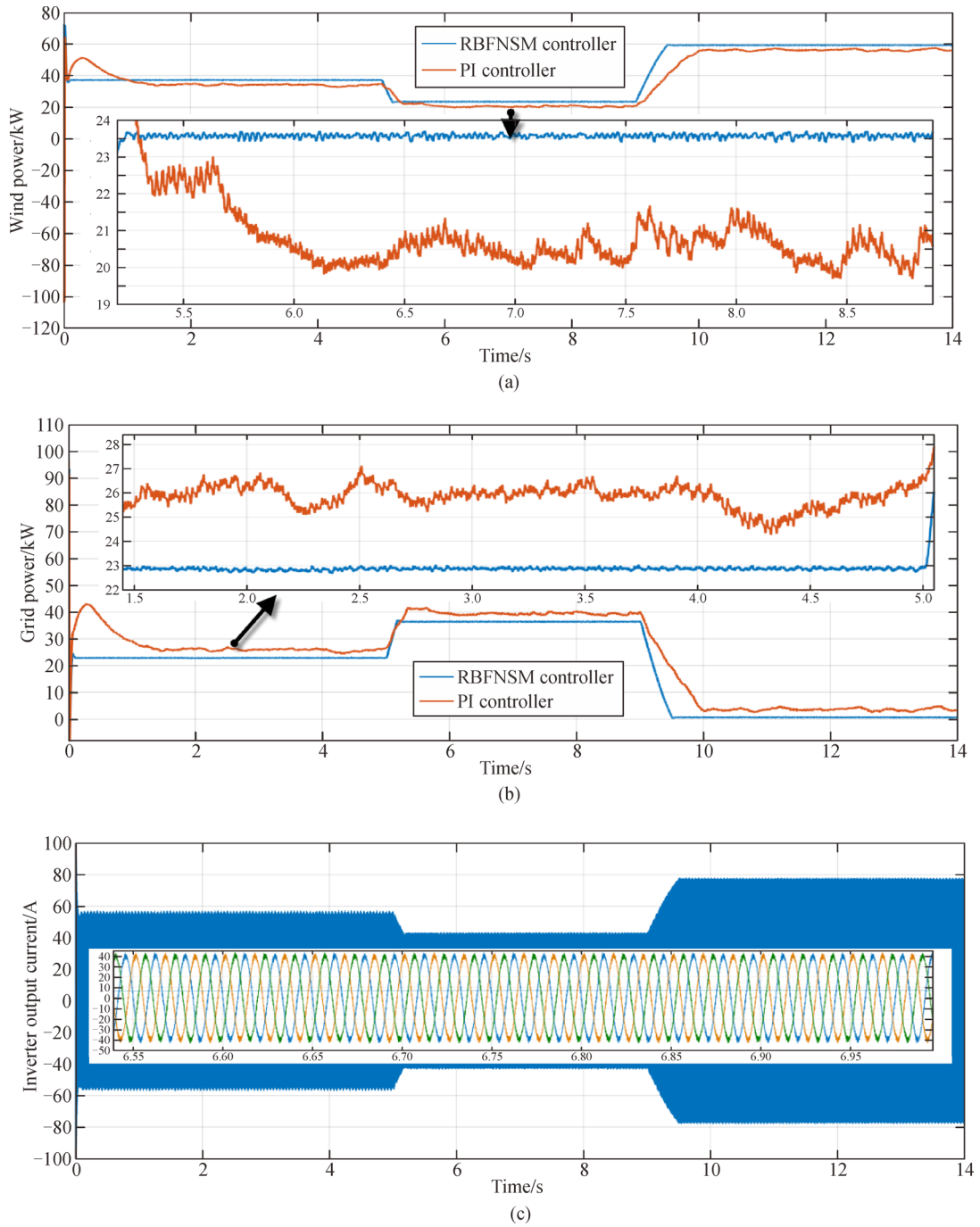


**Fig. 11** Simulated results for wind system in case 1

(a) Maximum power tracking response of the WT; (b) response of the grid power; (c) inverter out current of wind turbine

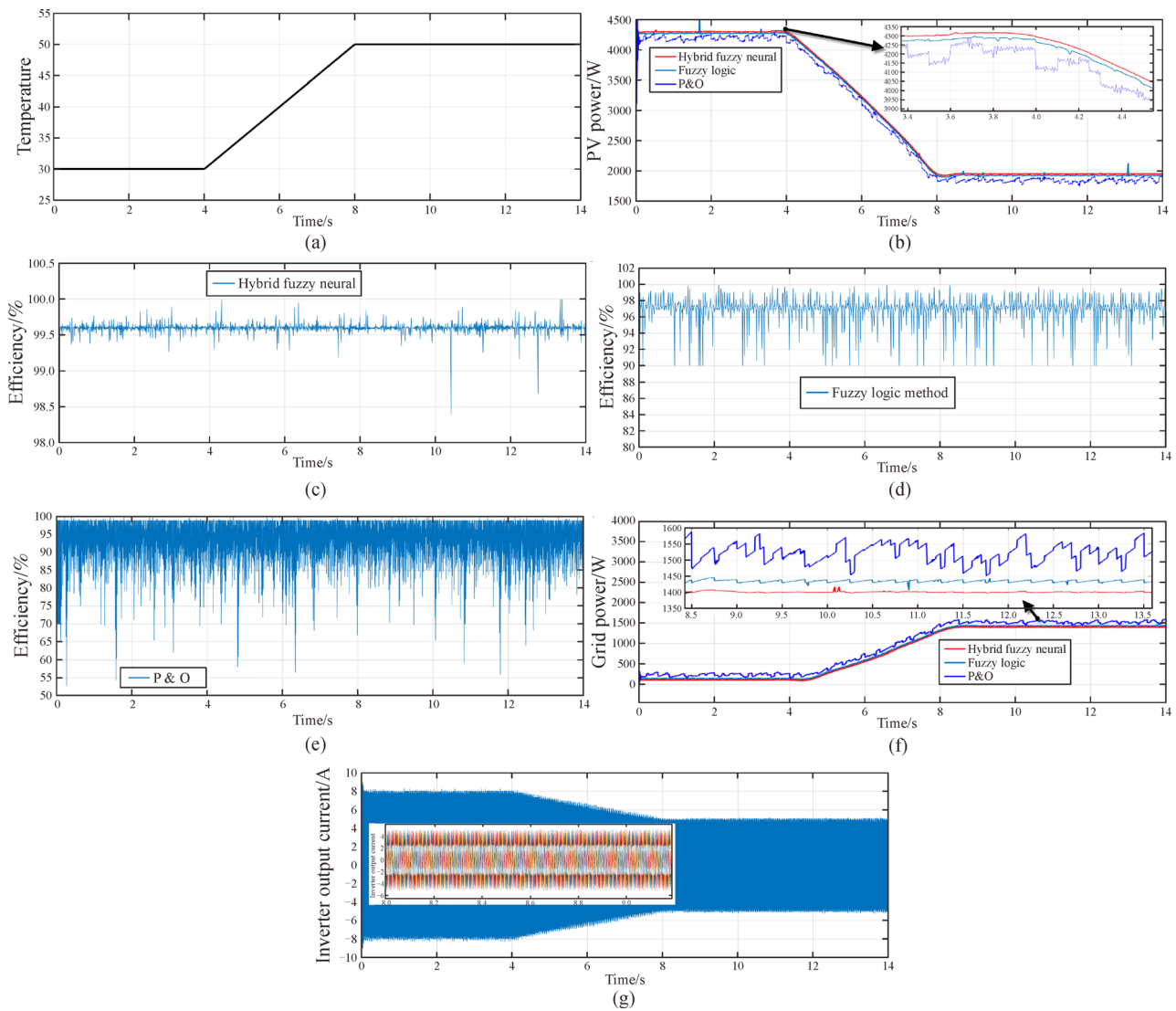


**Fig. 12** Simulated results of variations of irradiance in case 2

(a) Temperature variations; (b) output power of PV system; (c) tracking efficiency of hybrid fuzzy-neural; (d) tracking efficiency of FLC; (e) tracking efficiency of P&O; (f) grid power; (g) inverter output current

**Table 6** Tracking efficiency and response time comparison for different MPPT techniques under temperature variation

Algorithm	Tracking efficiency (avg)	Response time (avg)/s	Oscillation around MPP (avg)/W
Hybrid fuzzy-neural	99.45	0.14	2.12
Fuzzy logic	97.62	0.19	7.21
P&O	94.84	0.27	26.12

**Table 7** Output power values of solar array in various temperature conditions

Time/s	Real value/W	Hybrid fuzzy-neural/W	Fuzzy logic/W	P&O/W
0–4	4298	4297	4261	4246
8–14	1952	1949	1904	1887

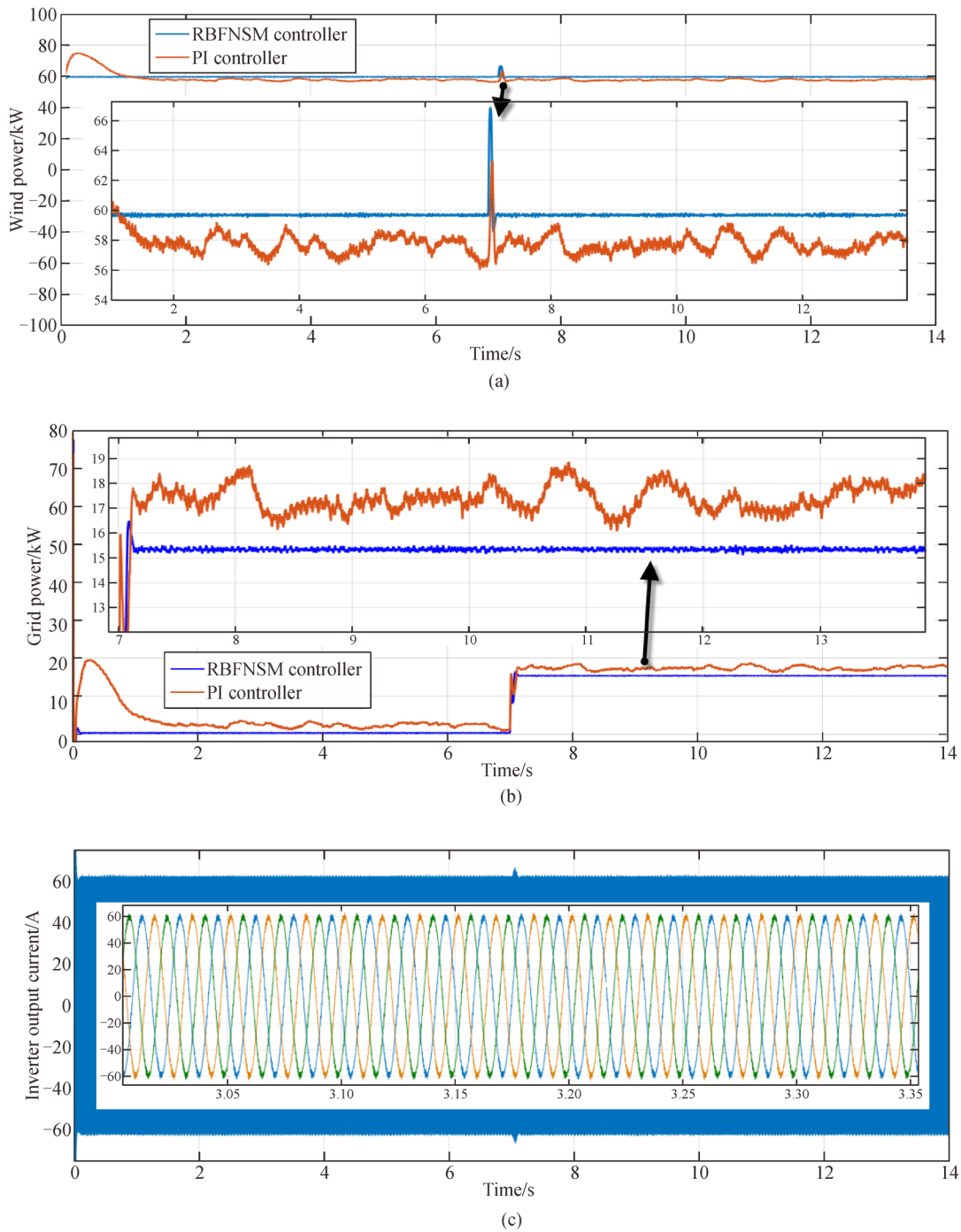


**Fig. 13** Simulated results for wind system in case 2

(a) Maximum power tracking response of the WT; (b) response of the grid power; (c) Inverter out current of wind turbine

**Table 8** Performance comparison of RBFNSM and PI Controller

Controller type	Wind speed/( $m \cdot s^{-1}$ )	Power coefficient ( $C_p$ )	Pitch angle/( $^\circ$ )	Average power/kW
RBFNSM	12	0.475	-0.09	59.2
PI	12	0.461	-0.66	58.1

## References

1. Rezvani A, Gandomkar M, Izadbakhsh M, Ahmadi A. Environmental/economic scheduling of a micro-grid with renewable energy resources. *Journal of Cleaner Production*, 2015, 87: 216–226
2. Izadbakhsh M, Gandomkar M, Rezvani A, Ahmadi A. Short-term resource scheduling of a renewable energy based micro grid. *Renewable Energy*, 2015, 75: 598–606
3. Rezvani A, Izadbakhsh M, Gandomkar M. Microgrid dynamic responses enhancement using artificial neural network-genetic algorithm for photovoltaic system and fuzzy controller for high wind speeds. *International Journal of Numerical Modeling, Electronic Networks, Devices and Fields*, 2015, 40(40): C7-415–C7-416
4. Rezvani A, Izadbakhsh M, Gandomkar M. Enhancement of microgrid dynamic responses under fault conditions using artificial neural network for fast changes of photovoltaic radiation and FLC for wind turbine. *Energy Systems*, 2015, 6(4): 551–584
5. Vafaei S, Gandomkar M, Rezvani A, Izadbakhsh M. Enhancement of grid-connected photovoltaic system using ANFIS-GA under different circumstances. *Frontiers in Energy*, 2015, 9(3): 322–334
6. Morimoto S, Nakayama H, Sanada M, Takeda Y. Sensorless output maximization control for variable-speed wind generation system using IPMSG. *IEEE Transactions on Industry Applications*, 2005, 41(1): 60–67
7. Ming C M, Chen C H. Intelligent control of a grid-connected wind-photovoltaic hybrid power systems. *Electrical Power and Energy Systems*, 2014, 55(2): 554–561
8. Algazar M M, Al-Monier H, EL-halim H A, Salem M E E K. Maximum power point tracking using fuzzy logic control. *International Journal of Electrical Power & Energy Systems*, 2012, 39(1): 21–28
9. Liu C, Wu B, Cheung R. Advanced algorithm for MPPT control of photovoltaic systems. In: *Proceeding of the Canadian Solar Buildings Conference*. Montreal, Canada, 2004
10. Rai A K, Kaushika N D, Singh B, Agarwal N. Simulation model of ANN based maximum power point tracking controller for solar PV system. *Solar Energy Materials and Solar Cells*, 2011, 95(2): 773–778
11. Chaouachi A, Kamel R M, Nagasaka K. A novel multi-model neuro-fuzzy-based MPPT for three-phase grid-connected photovoltaic system. *Solar Energy*, 2010, 84(12): 2219–2229
12. Kharb R K, Shimi S L, Chatterji S, Ansari M F. Modeling of solar PV module and maximum power point tracking using ANFIS. *Renewable and Sustainable Energy*, 2014, 33(5): 602–612
13. Afsin A, Kulaksiz A. Training data optimization for ANNs using genetic algorithms to enhance MPPT efficiency of a stand-alone PV system. *Turkish Journal of Electrical Engineering and Computer Sciences*, 2012, 20(2): 241–254
14. Ben Salah C, Ouali M. Comparison of fuzzy logic and neural network in maximum power point tracker for PV systems. *Electric Power Systems Research*, 2011, 81(1): 43–50
15. Rezvani A, Izadbakhsh M, Gandomkar M. Enhancement of hybrid dynamic performance using ANFIS for fast varying solar radiation and fuzzy logic controller in high speeds wind. *Journal of Electrical Systems*, 2015, 11(1): 11–26
16. Vinchek R M, Kargar A, Markadeh G A. A hybrid control method for maximum power point tracking (MPPT) in photovoltaic systems. *Arabian Journal for Science and Engineering*, 2014, 39(6): 4715–4725
17. Izadbakhsh M, Rezvani A, Gandomkar M. Improvement of microgrid dynamic performance under fault circumstances using ANFIS for fast varying solar radiation and fuzzy logic controller for wind system. *Archives of Electrical Engineering*, 2014, 63(4): 551–578
18. Hadji S, Krim F, Gaubert J P. Development of an algorithm of maximum power point tracking for photovoltaic systems using genetic algorithms. In: *7th International Workshop on Systems, Signal Processing and their Applications (WOSSPA)*. 2011, 43–46
19. Bakić V, Pezo M, Stevanović Žana, Živković M, Grubor B. Dynamical simulation of PV/Wind hybrid energy conversion system. *Energy*, 2012, 45(1): 324–328
20. Samia S, Ahmed G. Modeling and simulation of hybrid systems PV/Wind/Battery connected to the grid. *International Conference of Automatic Control*, Nantou, Taiwan, China, 2013
21. Samrat N H, Ahmad N B, Choudhury I A, Taha Z B. Modeling, control, and simulation of battery storage photovoltaic-wave energy hybrid renewable power generation systems for island electrification in Malaysia. *Scientific World Journal*, 2014, 2014(38): 278–279
22. Bhandari B, Poudel S R, Lee K T, Ahn S H. Mathematical modeling of hybrid renewable energy system: a review on small hydro-solar-wind power generation. *International Journal of Precision Engineering and Manufacturing-green Technology*, 2014, 1(2): 157–173
23. Ahmed J, Salam Z. An improved perturb and observe (P&O) maximum power point tracking (MPPT) algorithm for higher efficiency. *Applied Energy*, 2015, 150: 97–108
24. Chen P C, Chen P Y, Liu Y, Chen J H, Luo Y F. A comparative study on maximum power point tracking techniques for photovoltaic generation systems operating under fast changing environments. *Solar Energy*, 2015, 119: 261–276
25. Lin W M, Hong C M. A new Elman neural network-based control algorithm for adjustable-pitch variable speed wind energy conversion systems. *IEEE Transactions on Power Electronics*, 2011, 26(2): 473–481
26. Lin S C, Chen Y Y. RBF network based sliding mode control. *IEEE International Conference on Systems*, 1994, 2(2): 1957–1961
27. Blaabjerg F, Teodorescu R, Liserre M, Timbus A V. Overview of control and grid synchronization for distributed power generation systems. *IEEE Transactions on Industrial Electronics*, 2006, 53(5): 1398–1409